

ARTICLE TYPE

Multivariate cluster point process to quantify and explore multi-entity configurations: Application to biofilm image data

Suman Majumder*¹ | Brent A. Coull² | Jessica L. Mark Welch³ | Patrick J. La Riviere⁴ | Floyd E. Dewhirst³ | Jacqueline R. Starr^{0,5} | Kyu Ha Lee^{0,2}

¹University of Missouri, Missouri, USA

²Harvard T.H. Chan School of Public Health, Massachusetts, USA

³Forsyth Institute, Massachusetts, USA

⁴University of Chicago, Illinois, USA

⁵Brigham and Women's Hospital, Massachusetts, USA

Correspondence

*Suman Majumder, University of Missouri.
Email: sm8qr@missouri.edu

Abstract

Clusters of similar or dissimilar objects are encountered in many fields. Frequently used approaches treat each cluster's central object as latent. Yet, often objects of one or more types cluster around objects of another type. Such arrangements are common in biomedical images of cells, in which nearby cell types likely interact. Quantifying spatial relationships may elucidate biological mechanisms. Parent-offspring statistical frameworks can be usefully applied even when central objects ("parents") differ from peripheral ones ("offspring"). We propose the novel multivariate cluster point process (MCP) to quantify multi-object (e.g., multi-cellular) arrangements. Unlike commonly used approaches, the MCP exploits locations of the central parent object in clusters. It accounts for possibly multilayered, multivariate clustering. The model formulation requires specification of which object types function as cluster centers and which reside peripherally. If such information is unknown, the relative roles of object types may be explored by comparing fit of different models via the deviance information criterion (DIC). In simulated data, we compared a series of models' DIC; the MCP correctly identified simulated relationships. It also produced more accurate and precise parameter estimates than the classical univariate Neyman-Scott process model. We also used the MCP to quantify proposed configurations and explore new ones in human dental plaque biofilm image data. MCP models quantified simultaneous clustering of *Streptococcus* and *Porphyromonas* around *Corynebacterium* and of *Pasteurellaceae* around *Streptococcus* and successfully captured hypothesized structures for all taxa. Further exploration suggested the presence of clustering between *Fusobacterium* and *Leptotrichia*, a previously unreported relationship.

KEYWORDS:

Imaging; Microbiome; Parent-offspring model; Plaque; Spatial statistics; Thomas process.

1 | INTRODUCTION

Instances abound in nature where one type of object is dispersed around another type of object. At interplanetary and field ecologic scales, respectively, radio galaxies^{1,2} and forest songbirds³ exemplify spatial clustering. At microscopic scales, among

⁰Co-senior authors

human cells and single-celled organisms, such arrangements are common. For example, hair cell development in the inner ear depends on surrounding support cells⁴, neurons generally require various adjacent support cells⁵, granulomatous lesions of the lung exhibit concentric rings of different cell types⁶, and platelets aggregate around red blood cells during clot formation, which can also involve other cell types. To describe and quantify such arrangements, we have developed a new multivariate cluster point process model (MCP). We also developed a procedure for using the MCP to explore possible clustering relationships not known *a priori*. In human dental plaque biofilm, spherical *Streptococcus* cells often cluster around the ends of filamentous *Corynebacterium* cells^{7,8}. These corn-cob-like arrangements have been observed for decades and likely hold clues about microbial interactions that can affect human health. We assessed performance of the MCP through simulations and by application to dental plaque biofilm image data.

Most biofilm image analysis approaches have focused on macro-level structural characteristics or derived features, such as biofilm volume, thickness, or surface roughness^{9,10}. Less commonly, spatial point process models have been used to analyze the spatial patterning of microbial cells: how cells of one taxonomic class (or taxon) are distributed in relation to other cells of the same or different taxa. However, standard point process models, such as the log-Gaussian Cox process model¹¹, do not account for the complex spatial clustering arrangements often present in biofilm images. Methods that can account for such complexity are needed to quantify visible arrangements and to explore and quantify spatially dependent arrangements that, unlike the “corn-cobs”, are not visually discernable. Quantification, in turn, would allow benchmarking and hypothesis testing, such as for comparing effects of an antibacterial treatment on biofilm architecture.

The Neyman-Scott process model (NSP)¹² is a classic statistical model used to quantify spatially dependent clustering relationships, most often applied to actual parents and offspring (such as trees in a forest). In this approach, locations of the central object in each cluster are treated as latent, in part because in a cluster comprising similar objects (such as a grove of trees or a school of fish), it may be impossible to identify any true parent individuals. In contrast, in corn-cob arrangements in dental plaque biofilm, the locations of the central cells are often known. Though reasonable for within-taxon clustering, naïve application of the NSP model to investigate between-taxon relationships is inappropriate because it ignores the taxon in the center of the clusters.

Corn-cob arrangements in dental plaque biofilm have other characteristics that preclude direct application of the NSP model or the related shot noise Cox process model¹³. First, the “parent” (i.e., central) and “offspring” (i.e., peripheral) cells are of different bacterial taxa, thus requiring a multivariate extension of univariate approaches. Though others have considered point process models for multi-type spatial data^{14,11,15,16}, we are unaware of any work addressing more complex clustering arrangements as a specific focus of model development. Second, the corn-cob arrangements sometimes include multiple “offspring” taxa in that both *Streptococcus* and *Porphyromonas* are observed around *Corynebacterium* “parents.” Existing multivariate cluster point process models^{17,18} can not model the taxon in the cluster center and have no scope to enforce multiple offspring taxa’s having the same parent taxon.

¹⁹ propose a multivariate clustering process model that permits multiple types of offspring to be clustered around the center. In the proposed configuration, however, any offspring can be affected by all potential cluster centers. Thus these models fail to exploit biological knowledge about which taxa are parents to which other offspring taxa. Further, parent processes are considered as fixed, known quantities and are not explicitly modeled. To our knowledge, existing approaches fail to address a third challenge, that the corn-cobs can be multilayered in nature (e.g., Figure 1). Fourth, the corn-cob arrangements themselves are part of a more complexly organized community that includes other taxa unrelated to the arrangements. None of the aforementioned methods address this challenge. Fifth, clustering configurations are not always known *a priori*. When configurations are known, the analysis goal might be to quantify them; in other instances the goal might be to explore the possible existence of clustering relationships.

The primary innovation of the proposed MCP model is that it exploits the known locations of central objects in clusters. It also addresses the above-described challenges together. Specifically, it can simultaneously quantify multivariate and multilayered clustering and inter-process relationships. The MCP is flexible in that it can simultaneously model clustered and non-clustered processes and can be applied in multivariate (multi-taxon) or univariate (individual taxon) contexts. It may seem restrictive that fitting the MCP model requires specification of which objects are central to clusters and which peripherally located. We demonstrate that the MCP can also be used to explore and infer the presence of newly proposed relationships by comparing model fit via the deviance information criterion (DIC). In this paper, we describe the model in detail, evaluate its performance through simulation studies, and demonstrate the feasibility of applying the model to both real and synthetic datasets.

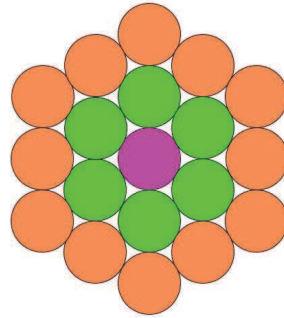


FIGURE 1 A multi-layered parent-offspring structure. The green dots behave as offspring to the pink dot while the orange dots behave as offspring to the green dots

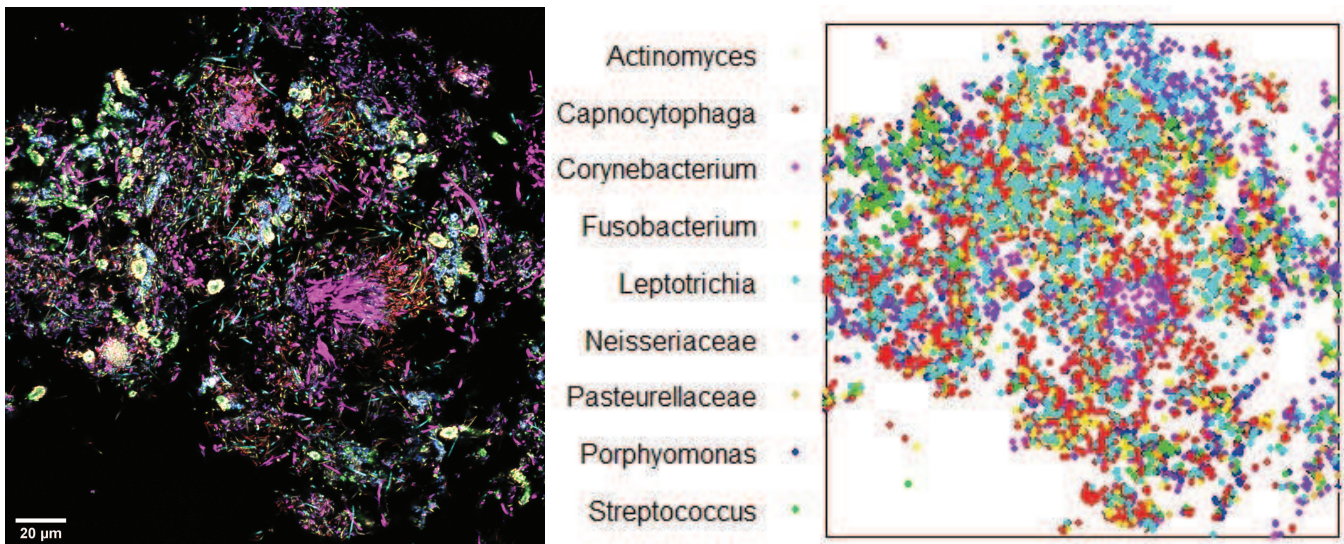


FIGURE 2 (a) A biofilm image of a dental plaque sample from from a human donor: RGB image - taxa relevant to the multi-layered concob arrangements are *Corynebacterium* (Pink), *Streptococcus* (Green), *Porphyromonas* (Blue) and *Pasteurellaceae* (Orange); (b) post-segmentation spatial locations of the centroids of cells identified via genus-specific probes, as indicated

2 | MICROBIOME BIOFILM IMAGE DATA FROM DENTAL PLAQUE SAMPLES

In this section, we present image data that motivate development of the method and that we analyzed by applying the MCP. These data and their collection methods and processing have been described in detail elsewhere⁸. Briefly, dental plaque samples were collected, embedded in methacrylate, sectioned, and subjected to multi-spectral fluorescence *in situ* hybridization (FISH) imaging. Multiple genus- and family-level probes were applied simultaneously to identify nine taxa. The near-universal probe Eub338 targeting most bacteria was also included (Figure 2 (a)). We performed segmentation of the biofilm image in FIJI²⁰ by applying a 3×3 median filter and the “Auto Local” thresholding function with the Bersen method. Spatial coordinate information for each cell’s centroid was generated by applying the “Analyze Particles” function with size filter of 0.5 μm diameter in FIJI (Figure 2 (b)).

The sampled image is representative of similar samples from the same and other donors without active tooth decay (not shown). Filamentous *Corynebacterium* cells (Figure 3 , pink) are common. Members of this genus are now believed to help establish the “healthy” dental microbiota, providing a scaffold around which other community members assemble. Some *Streptococcus* (Figure 3 , green) and/or *Porphyromonas* (Figure 3 , blue) cells surround the tips of *Corynebacterium* filaments⁸.

Adding another layer and further complexity, *Pasteurellaceae* cells (Figure 3, orange) sometimes surround *Streptococcus* cells^{8,21}. As outlined in Section 1, these arrangements allow *Streptococcus* to serve as either parent, offspring, or both in the same cluster. Other taxa scatter seemingly homogeneously and may have additional spatial relationships with *Corynebacterium*, *Streptococcus*, *Porphyromonas*, or *Pasteurellaceae* (Supplementary Materials, Section B). Below, we demonstrate a procedure to explore previously undescribed patterns among these other taxa.

3 | MULTIVARIATE CLUSTER POINT PROCESS MODEL

We consider a multivariate process Y to be a collection of processes Y_i , $i = 1, \dots, m$, at location $\mathbf{s} \in \mathcal{W} \subset \mathbb{R}^2$, where each component Y_i is a Poisson process characterized by an intensity function $\lambda_i(\mathbf{s})$ and \mathcal{W} , the observation window. In application to the biofilm sample, each Y_i captures the spatial distribution of the i -th taxon.

3.1 | Model formulations

Suppose that Y_1, \dots, Y_p , are homogeneous Poisson processes (HPP) with intensities λ_v^C for $v = 1, \dots, p$ ($< m$), and they serve only as parent processes ("C" signifies central objects, or parents). Then we consider the q ($\leq m - p$) processes, Y_{p+1}, \dots, Y_{p+q} , that behave as offspring processes. Each offspring process is assumed to have one parent process. Let C_l for $l = p + 1, \dots, p + q$ denote the corresponding parent process for offspring process Y_l with the following properties:

- i) If offspring processes Y_l and $Y_{l'}$, $l \neq l'$ share a parent process, then $C_l = C_{l'}$;
- ii) If an offspring process Y_j serves as a parent process for another offspring process Y_l for some l and $j = p + 1, \dots, p + q$, then $C_l = Y_j$.

We assume that the offspring points are distributed around parent point $\mathbf{c} \in C_l$, $l \in \{p + 1, \dots, p + q\}$ according to the rule $\alpha_l k_l(\cdot - \mathbf{c}, h_l)$, where α_l is the average number of offspring per parent, $k_l(\cdot, \cdot)$ is a kernel (e.g. Gaussian, uniform or Cauchy), and h_l is a bandwidth parameter that controls the distance between the parent and its offspring locations for the l -th offspring process²². The remaining $m - p - q$ types (e.g. taxa) that are unrelated to multilayered arrangements are modeled as HPP with intensities λ_j for $j = p + q + 1, \dots, m$. Therefore, under the proposed specification, the intensity functions for the various processes are

$$\begin{aligned} \lambda_v(\mathbf{s}) &= \lambda_v^C, \quad v = 1, \dots, p, \quad \lambda_l(\mathbf{s}) = \alpha_l \sum_{\mathbf{c}_l \in C_l} k_l(\mathbf{s} - \mathbf{c}_l, h_l), \quad l = p + 1, \dots, p + q, \\ \lambda_j(\mathbf{s}) &= \lambda_j, \quad j = p + q + 1, \dots, m. \end{aligned} \quad (1)$$

Since the different processes are assumed to be conditionally independent of each other, the log-likelihood as a function of the unknown parameters, $\boldsymbol{\theta} = \{\alpha_{p+1}, \dots, \alpha_{p+q}, h_{p+1}, \dots, h_{p+q}, \lambda_1^C, \dots, \lambda_p^C, \lambda_{p+q+1}, \dots, \lambda_m\}$, is given by

$$\begin{aligned} l(Y|\boldsymbol{\theta}) &\propto |\mathcal{W}| - \sum_{v=1}^p |\mathcal{W}| \lambda_v^C - \sum_{l=p+1}^{p+q} \alpha_l \sum_{\mathbf{c}_l \in C_l} \int_{\mathcal{W}} k_l(\mathbf{u} - \mathbf{c}_l, h_l) d\mathbf{u} - \sum_{j=p+q+1}^m |\mathcal{W}| \lambda_j \\ &+ \sum_{v=1}^p n_v \log \lambda_v^C + \sum_{l=p+1}^{p+q} \sum_{\mathbf{y} \in Y_l} \log \left(\alpha_l \sum_{\mathbf{c}_l \in C_l} k_l(\mathbf{y} - \mathbf{c}_l, h_l) \right) + \sum_{j=p+q+1}^m n_j \log \lambda_j, \end{aligned} \quad (2)$$

where $|\mathcal{W}|$ is the area of \mathcal{W} , and n_i denotes the number of observations from the i -th process in \mathcal{W} .

3.2 | Quantities of interest

For a stationary point process, Ripley's $K(r)$ function²³ is defined as the expected number of neighbors located within distance r from a typical point, divided by the intensity of the process. Since some of the processes being modeled are non-stationary, we shall use K_{inhom} ²⁴, the inhomogeneous K -function. For either a homogeneous or inhomogeneous process i , we can estimate $K_i(r)$ by

$$\hat{K}_i(r) = \sum_{\mathbf{s}, \mathbf{u} \in Y_i} \frac{\mathbb{I}(0 < \|\mathbf{s} - \mathbf{u}\| \leq r)}{\lambda_i(\mathbf{s}; \hat{\boldsymbol{\theta}}_i) \lambda_i(\mathbf{u}; \hat{\boldsymbol{\theta}}_i)} w_{\mathbf{s}, \mathbf{u}} \quad (3)$$

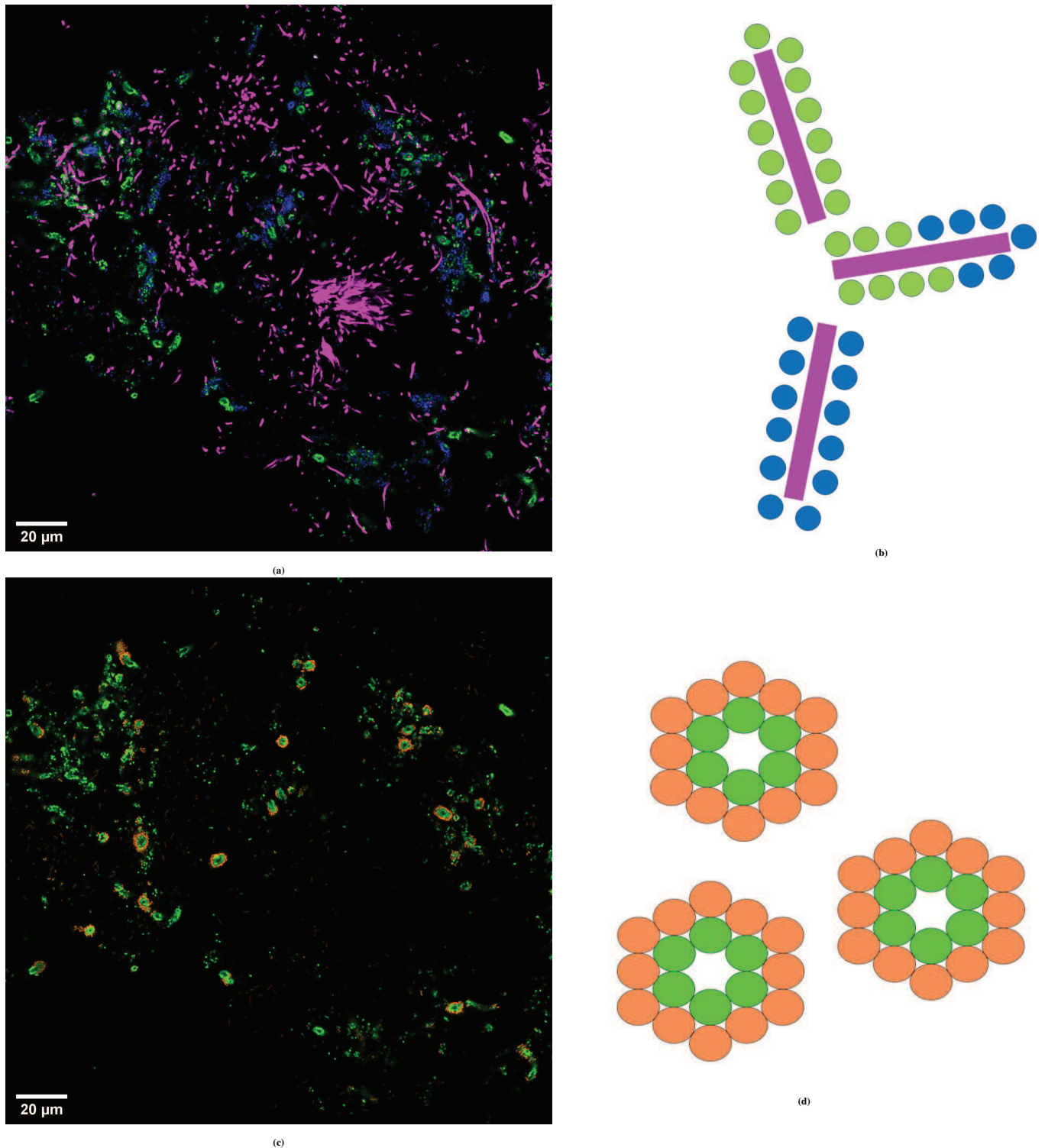


FIGURE 3 (a) The same image as in Figure 2 , displaying channels corresponding to *Corynebacterium* (Pink), *Streptococcus* (green) and *Porphyromonas* (Blue); (b) cartoon depicting various corn-cob structures visible in the image. The corn-cob structures are present in areas of the image corresponding to the tip of the *Corynebacterium*. At the center of the dense clump of *Corynebacterium* in (a), no corn-cobs are observed; (c) The same image as in Figure 2 , displaying channels corresponding to *Pasteurellaceae* (Orange) and *Streptococcus* (Green); and (d) a cartoon image illustrating the clustering of *Pasteurellaceae* around *Streptococcus*. Hiding the pink *Corynebacterium* channels highlights the outer layer in the multilayer arrangements. For other examples of biofilm images with corn-cob structures in which both *Streptococcus* and *Porphyromonas* cells cluster around the same *Corynebacterium* cell, see Supplemental Figure S2, panel C, in Mark Welch et al. (2016).

where $\hat{\theta}_i$ is the set of estimated parameters that control process i , and $w_{\mathbf{s}, \mathbf{u}}$ is the Ripley's edge-correction factor²⁵. For homogeneous point patterns, the estimate (3) is close to πr^2 for all values of r , and thus the estimated K -functions corresponding to Y_j , for $j = 1, \dots, p, p+q+1, \dots, m$ should be close to πr^2 . For inhomogeneous processes, the closed form expression is not evident, as is the case for processes Y_j for $j = p+1, \dots, p+q$.

By graphing the K -function, one can use it to assess homogeneity of processes. While it can thus be used to describe spatial patterns within a certain range, the K -function does not allow for quantitative validation of the point process models. Therefore, we interpret the MCPP model based on the individual model parameters, which, in turn, influence the estimated K -functions.

As outlined in Section 3.1, parameters of primary interest in the proposed model are the α_l and h_l parameters, for $l = p+1, \dots, p+q$. The offspring density parameter α_l corresponds to how densely the l -th process clusters around its parent process, with higher values indicating denser clustering. The bandwidth parameter, h_l determines how tightly the l -th process clusters around its parent process. A value of $h_l > h_0$ may indicate no or negligible clustering between the l -th process and its supposed parent process, where h_0 is a predetermined threshold based on domain knowledge from experts. Interpretation of h_l can change depending on choice of $k_l(\cdot, \cdot)$. For example, in a Gaussian or Cauchy kernel, h_l can be thought of as a scaled average distance between the offspring and parent, whereas in a uniform kernel, it represents the maximum distance between the parent and its offspring. Regardless of $k_l(\cdot, \cdot)$, one can also interpret h_l as a parameter that estimates the median distance between the parents and offsprings: $\frac{32}{27}h$, $\sqrt{5}h$ and $\frac{2}{3}h$ for Gaussian, Cauchy and uniform kernels respectively. These parameters provide additional quantitative information about the relationship between a clustered process and its parent process, quantities not captured by the $K(r)$ function.

3.3 | Prior distributions and practical considerations

We outline priors for the unknown model parameters to complete the Bayesian specification of the MCPP model. Specifically, we consider the following priors:

$$\begin{aligned} \alpha_l &\stackrel{iid}{\sim} \text{Gamma}(a_Y, b_Y), \quad h_l \stackrel{iid}{\sim} \text{Half-Normal}(\sigma), \quad l = p+1, \dots, p+q, \\ \lambda_v^C &\stackrel{iid}{\sim} \text{Gamma}(a_C, b_C), \quad v = 1, \dots, p, \quad \lambda_j \stackrel{iid}{\sim} \text{Gamma}(a, b), \quad j = p+q+1, \dots, m, \end{aligned} \quad (4)$$

where $\stackrel{iid}{\sim}$ denotes independent and identically distributed, and $(a, b, a_Y, b_Y, a_C, b_C, \sigma)$ are hyperparameters to be specified.

It is well appreciated that using a noninformative prior for spatial bandwidth or scale parameters is impossible due to numerical reasons, specifically, weak identifiability of the posterior distribution^{26,27,28}. We use a half-normal prior for the bandwidth parameters h_l ; ensuring the prior assigns mass to relatively small positive values, stabilizing the parameter estimation. Specifically, the value of hyperparameter σ can be set such that the 99-th percentile of the half-normal prior corresponds to the maximum distance d between a parent point and offspring points. This choice helps sensitize the proposed Bayesian framework to stronger clustering within a small radius, which is expected when, for example, cells of two bacterial taxa directly interact. In general, choosing the value of d should depend on the context.

3.4 | Computational scheme

Combining (2) and (4), the joint posterior density for the proposed MCPP model can be written as $\pi(\boldsymbol{\theta}|Y) \propto L(Y|\boldsymbol{\theta})\pi(\boldsymbol{\theta})$, where $\pi(\boldsymbol{\theta})$ is the product of all the individual prior densities. We then proceed to draw samples from the posterior distribution by using a Markov chain Monte Carlo (MCMC) algorithm. Conventional NSP-type approaches treat the number of parent points and their locations as random and thus require an additional reversible jump MCMC step to estimate the parameters associated with the latent parent process^{29,26}. In contrast, the proposed framework exploits the fact that the parent processes are observed and proceeds without a complex birth-death-move algorithm. The components of $\boldsymbol{\theta}$ can then be updated by Gibbs sampling (exploiting conjugacies in the full conditionals) or via Metropolis-Hastings steps (details in Section C of the Supplementary Material).

One practical challenge is that the integral term in (2) does not have a closed-form expression. Therefore, we use Monte Carlo methods to approximate the integral for computational efficiency. In practice, the expression $\int_{\mathcal{W}} k_l(\mathbf{u} - \mathbf{c}_l, h_l) d\mathbf{u}$ can be thought of as the probability of occurrence of \mathbf{X}_l within the observation window \mathcal{W} , where \mathbf{X}_l is a bivariate real-valued random variable with density $k_l(\cdot - \mathbf{c}_l, h_l)$. Furthermore, in the proposed framework with Thomas processes, $k_l(\cdot - \mathbf{c}_l, h_l)$ corresponds to a bivariate normal density function with mean \mathbf{c}_l and covariance matrix $h_l^2 \mathbf{I}$. In this case, we draw samples from the bivariate

normal distribution and compute the average proportion of points that fall within \mathcal{W} , which serves as an approximation to the integral term in (2).

We further optimized the code by using the C language. An R package is available in the online repository at <https://github.com/SumanM47/MCPP.git>. The implementation of the model in the R package can generate 10,000 scans in 1.5 minutes for a dataset with ~ 150 points from a single parent process with a total of ~ 750 points from two offspring processes on a Dell Latitude 7210 laptop with i5 cores and 16 gigabytes of memory.

3.5 | A metric to explore model configurations

Use of the MCPP model requires prespecification of parent-offspring arrangement. In practice, one may lack prior knowledge of intertaxon spatial clustering. One may suspect their existence, or one may simply seek to explore consistency of the data with one or more possible clustering arrangements. For this purpose, we propose a model validation method to identify a best-fitting model among a series of models specifying different possible clustering relationships. Specifically, we use the DIC³⁰ to compare models involving different parent-offspring structures and/or different kernels for the distribution of offspring around the parent. For example, models could be fit such that A is assumed to cluster around B in model 1, C around D in model 2, and both in model 3. The model with the smallest DIC would be identified as the best fit. This model comparison process enables use of the MCPP as an exploratory tool. Newly proposed clustering arrangements can be quantified and evaluated for consistency with the data.

3.6 | Goodness-of-fit

We also assess goodness-of-fit of the models by comparing the observed and estimated counts of different objects (in this case, taxa). Specifically, for the parent species, the estimated intensity parameter λ_v^C , $v = 1, \dots, p$, per unit area can be scaled by the area of the observation window. If the model is approximately correct, this quantity, $\lambda_v^C |W|$, should be close to the number of v -th parent cells counted in the observation window. For approximating the l -th offspring count, one can compute the posterior mean of $\alpha_l \sum_{\mathbf{c} \in C_l} \int_W k_l(\mathbf{u} - \mathbf{c}, h_l) d\mathbf{u}$ for $l = p+1, \dots, p+q$. The integral term can be approximated by Monte Carlo methods as described in Section 3.4. This expression involves both the offspring density parameter and the bandwidth parameter and therefore helps validate the joint estimate of the (α_l, h_l) pair. In our example, $\lambda^C |W|$ should provide a good estimate of the number of *Corynebacterium* cells; and $\alpha_2 \sum_{\mathbf{c} \in C_2} \int_W k_2(\mathbf{u} - \mathbf{c}, h_2) d\mathbf{u}$, $\alpha_3 \sum_{\mathbf{c} \in C_3} \int_W k_3(\mathbf{u} - \mathbf{c}, h_3) d\mathbf{u}$ and $\alpha_4 \sum_{\mathbf{c} \in C_4} \int_W k_4(\mathbf{u} - \mathbf{c}, h_4) d\mathbf{u}$ should be close to the observed number of *Streptococcus* clustered around *Corynebacterium*, the observed number of *Porphyrromonas* clustered around *Corynebacterium*, and the observed number of *Pasteurellaceae* clustered around *Streptococcus*, respectively.

4 | SIMULATION STUDIES

We performed two types of simulation studies to benchmark the performance of the method as an inference tool and as an exploratory tool. The first simulation study was designed to assess performance of the MCPP when the true parent-offspring relationships are known and to compare its performance to that of an existing method, the NSP. The second study was designed to assess the MCPP's performance in ranking the fit of models parameterizing different proposed parent-offspring relationships and different kernels, and in identifying the best-fitting model. In both types of studies, we compared the estimated and true parameter values under the generating model.

4.1 | Simulation I: Comparative performance for quantifying a prespecified configuration

4.1.1 | Simulation set-up

For simplicity, the unit square was taken as the observation window. We generated data under the model outlined in Section 3, with $q = 2$ offspring taxa B and C around the same parent taxon A , which was the only parent taxon ($p = 1$). We considered twelve data scenarios (Supplementary Material Table S.1) that varied in terms of offspring density (α_2, α_3) being 'Sparse', 'Dense' or 'Mixed'; bandwidth (h_2, h_3) being 'Low' or 'High'; and presence or absence of a taxon spatially unrelated to the multilayered arrangement (hereinafter referred to as "unrelated" taxon). Throughout the scenarios, the intensity of the parent

process (λ_1^C) and that of the process for the unrelated taxon (λ_4) were set to 150 and 95, respectively. For each of the twelve scenarios, we generated 100 images, each analyzed as an independent dataset.

4.1.2 | Analysis plan and hyperparameters

We applied the following approaches to each simulated dataset:

- (i) *MCP*: Multi-offspring taxa (A as the parent of B or C) were jointly analyzed in one framework by using the MCP.
- (ii) *NSP*: Ignoring the parent taxon A , only offspring taxa B and C were analyzed separately (by necessity, with the NSP). We applied the method of minimum contrast²⁷, by using the R package `spatstat`³¹.

The parameters estimated by the two approaches have different interpretations. For example, the bandwidth parameter h_2 in NSP models from analysis (ii) is interpreted as the distance scale for the unobserved cluster formed by offspring taxon B , ignoring the observed parent taxon A . Despite this distinction, we included analysis (ii) using the NSP because it is among the most relevant cluster point process models applied to this class of problems. In simulation studies, we primarily focused on the numerical performance of the methods in estimating the parameters rather than on their interpretations. We do not provide estimates of the K -functions because a) the data were generated under the homogeneity assumption and b) the K -function is a graphical inspection tool and cannot be used to summarize performance over multiple datasets.

For analysis (i), we set the hyperparameters (a_Y, b_Y, a_C, b_C, a, b) to 0.01. We set the hyperparameter σ to 0.02 so that the 99-th percentile of the prior distribution of h_1 's was approximately 0.05 (i.e. 5% of the length of the observation window). We used the posterior means as point estimates of the model parameters.

We estimated the offspring intensity (α_2, α_3) and bandwidth parameters (h_2, h_3) for the offspring processes (taxa B and C) and the intensity parameter (λ_1^C) for the parent process (taxon A). For the MCP, the presented statistics are the average of the posterior mean for the parameters for each of the datasets in a given scenario. We also computed the posterior standard deviation (SD) averaged over the 100 datasets for each scenario and the standard deviations of the posterior means of the estimates for the different datasets (SD_{EST}). With the NSP, no uncertainty measure is available for the individual estimates for each dataset, so we computed only the standard deviation of each estimate across the datasets. For each scenario, we report the percentage of datasets in which the NSP failed to converge and computed average estimates and SEs based only on the datasets in which the model converged.

4.1.3 | Primary results

The MCP method performed well in estimating the true parameter values, with both a small SD and a small SD_{EST} (Tables 1 and S.2 of Supplementary Materials). The NSP method often failed to converge, in up to 70% of datasets, depending on the scenario. When the NSP did converge, it produced results that were nonsensical, with SEs too high to give any credibility to these estimates.

For both methods, standard errors increased in the high-bandwidth scenarios compared with the low-bandwidth scenarios. The parent process intensities were also captured better by the MCP than by the NSP, especially in high-bandwidth scenarios. Lastly, performance of the MCP approach was not affected by the presence of a taxon spatially unrelated to the multilayered arrangement (Tables 1 and S.2 of Supplementary Materials).

4.1.4 | Sensitivity analyses

As explained in Section 3.3, we used a half-normal prior for the bandwidth parameter. We conducted comprehensive sensitivity analyses (Supplementary Materials, Section E) to examine sensitivity of conclusions to the choice of prior distribution for the bandwidth parameter: half-normal, uniform, or log-normal. In summary, the proposed framework was not sensitive to the choice of the prior distribution for the bandwidth parameter in scenarios with low bandwidth. In high-bandwidth scenarios, however, elicitation of an informative prior seemed to help the proposed framework become more numerically stable, increasing **precision**.

TABLE 1 The true value, estimates (EST), and uncertainty measures for the offspring density (α_2, α_3), bandwidth (h_2, h_3), and parent process (λ^C) parameters from the MCPP and NSP analyses in the first six simulated scenarios (those without any unrelated taxon). For the MCPP model, the estimates are the posterior means averaged over different datasets, the SD is computed by averaging the posterior standard deviation over different datasets, and the SD_{EST} is computed as the standard deviation of the estimates over the datasets. For the NSP model, the estimates are the outputs of the minimum contrast method, and SE is calculated similarly by using these estimates. The SD for the NSP model is not computed, as the method does not provide an uncertainty measure. The last column (%F) refers to the percentage of datasets in which the NSP model failed to converge for a given scenario.

Scenario		True value	MCPP			NSP		
			EST	SD	SD_{EST}	EST	SE	%F
1	α_2	1.50	1.54	0.10	0.11	2.34	7.71	6
	α_3	1.00	1.03	0.08	0.09	1.97	6.84	
	h_2	0.01	0.01	< 0.01	< 0.01	0.01	0.04	
	h_3	0.02	0.02	< 0.01	< 0.01	0.70	6.43	
	λ_1^C	150.00	164.07	13.16	13.28	170.78	52.51	
2	α_2	1.50	1.50	0.11	0.11	291.16	383.69	26
	α_3	1.00	1.02	0.08	0.08	1.06	0.40	
	h_2	0.10	0.08	0.01	0.01	8.33	23.82	
	h_3	0.01	0.01	< 0.01	< 0.01	0.01	< 0.01	
	λ_1^C	150.00	162.74	13.05	13.52	679.72	2378.68	
3	α_2	4.00	4.05	0.14	0.16	13.30	66.75	1
	α_3	3.00	3.06	0.13	0.11	10.60	75.03	
	h_2	0.01	0.01	< 0.01	< 0.01	0.02	0.10	
	h_3	0.02	0.02	< 0.01	< 0.01	0.03	0.08	
	λ_1^C	150.00	204.84	14.50	14.29	209.22	49.75	
4	α_2	4.00	4.01	0.17	0.17	710.62	648.03	56
	α_3	3.00	3.04	0.13	0.12	3.00	0.62	
	h_2	0.10	0.09	0.01	0.01	1.21	0.77	
	h_3	0.01	0.01	< 0.01	< 0.01	0.01	< 0.01	
	λ_1^C	150.00	202.08	14.34	15.32	20.33	45.79	
5	α_2	4.00	4.05	0.15	0.16	4.07	0.68	1
	α_3	1.00	1.03	0.17	0.09	3.06	14.91	
	h_2	0.01	0.01	< 0.01	< 0.01	0.01	< 0.01	
	h_3	0.02	0.02	< 0.01	< 0.01	1.10	10.15	
	λ_1^C	150.00	203.82	14.51	15.40	203.47	35.16	
6	α_2	4.00	4.02	0.17	0.14	685.54	694.99	53
	α_3	1.00	1.01	0.07	0.06	2.49	10.25	
	h_2	0.10	0.09	0.01	0.01	1.48	1.21	
	h_3	0.01	0.01	< 0.01	< 0.01	0.02	0.07	
	λ_1^C	150.00	198.19	14.22	13.86	35.99	99.33	

4.2 | Simulation II: Evaluating model selection

4.2.1 | Simulation set-up

The proposed MCPP model requires specification of the relationships one wishes to quantify and the offspring distribution kernel. This simulation study was designed to assess identification of the true model and to compare estimated parameters to the true model parameters. The unit square was taken as the observation window. We generated data under the model outlined in Section 3, with $q = 2$ offspring taxa B and C around the same parent taxon A , which was the only parent taxon ($p = 1$), and $m = 4$ by producing an extra unrelated taxon D . We considered 4 different scenarios that differed in the choice of $k_l(\cdot, \cdot)$ (Gaussian or Cauchy) and in the magnitude of h_l (0.01 or 0.05). We generated 100 datasets for each of the four scenarios. The

intensity functions for A and D were set to 150 and 100, respectively, and (α_1, α_2) was set to (2, 1.5) in all the scenarios. Since the bandwidth parameters most strongly affect inference (Table 1), we focus our analysis on scenarios with varying h_j .

4.2.2 | Analysis plan and hyperparameters

We represent a parent-offspring relationship between taxa A and B by $A \rightarrow B$, with the arrow directed from the parent towards the offspring. If parent A has two offsprings B and C , it is denoted by $A \rightarrow BC$. Different parent-offspring relationships within the same model are separated by $:$. $A \rightarrow BC : D \rightarrow E$ denotes that A is a parent to B and C and D a parent to E . The parent-offspring relationships in the true model are represented as $A \rightarrow BC$. Any taxa not represented in the notation and present in the model are modeled as independent HPP (e.g., taxon D). We denote the kernels used for the model, whether Gaussian ($k^{(G)}$), Cauchy ($k^{(C)}$) or Uniform ($k^{(U)}$), by hyphenation. $A \rightarrow BC-k^{(G)}$ and $A \rightarrow BC-k^{(C)}$ denote the two true models for this simulation.

We generated data from the two true models under low and high bandwidth parameter settings. For each of these four types of scenarios, we fit 9 different models for each dataset by varying the parent-offspring relationships presented in the model ($A \rightarrow BC$, $A \rightarrow B$, and $A \rightarrow B : D \rightarrow C$) and the choice of kernels ($k^{(G)}$, $k^{(C)}$, and $k^{(U)}$). For each scenario, the model that most often had the lowest DIC was considered the best fit. We obtained parameter estimates based on this model.

We set the hyperparameters a_Y , b_Y , a_C , b_C , a , b , and σ to the same value as in Section 4.1.2 and estimated the same quantities of interest in the same manner.

4.2.3 | Primary results

Use of the DIC successfully identified true parent-offspring arrangements for all datasets in all scenarios. Regarding kernel selection, in some scenarios the approach did not select the correct kernel used to generate the data (Table 2). This was particularly so with high bandwidth parameters. This discrepancy did not greatly affect the method's performance, which was excellent for all four data-generating mechanisms (Table 2). However, the estimated median distances between the parent offspring ($\frac{32}{27}h$ for Gaussian and $\sqrt{5}h$ for Cauchy) are similar under the scenarios with high bandwidth parameters, indicating the robustness of MCPP to the choice of kernel.

5 | ANALYSIS OF HUMAN MICROBIOME BIOFILM IMAGE DATA

As another way to illustrate use of the proposed MCPP, we analyzed the microbial biofilm image data described in Section 2. One challenge of biofilm image data is higher-order spatial structure, such as is evident in the image of a dental plaque biofilm community. Among other reasons for macro-level community structure, the environment at the outer edge of dental biofilm differs from that near the tooth surface. More locally, *Streptococcus* and *Porphyromonas* cluster around *Corynebacterium* only at its tip, not along its length and not at its base Figure 3 and⁸. Image sampling and processing further contribute to heterogeneity, especially in that the image is of a two-dimensional slice from a three-dimensional structure. Some areas of the image have a higher concentration of cross-sections in which *Corynebacterium* cells themselves appear spherical, whereas other areas display large numbers of lengthwise *Corynebacterium* filaments. Though some relationships are well known, there are undoubtedly intertaxon relationships that are yet unexplored and undocumented. Our method presents an opportunity to explore different possible relationships. With these objectives in mind, we performed two different analyses on this sample. In the first, we considered only the parent-offspring-type clustering configurations that have already been established.^{7,8,21} We analyzed data from the whole image and data from the same image divided into four quadrants, each with more homogeneous spatial patterns than the whole. In the second analysis, we explored various possible clustering configurations along with those considered in the first analysis; we evaluated consistency of these new structures with the data, i.e. their plausibility based on model fit.

TABLE 2 Estimates (EST) and uncertainty in the estimates (SD and SD_{EST}) for the model parameters for the selected (best fit) model across four simulation scenarios outlined in Section 4.2. Fitted models are represented by hyphenated combination of different arrangements ($A \rightarrow BC$, $A \rightarrow B$ or $A \rightarrow B; D \rightarrow C$) and different offspring kernels ($k^{(G)}$, $k^{(C)}$ or $k^{(U)}$). Data generation scenario is denoted by hyphenated combination of offspring kernel ($k^{(G)}$ or $k^{(C)}$) and the arrangement ($A \rightarrow BC$) with the bandwidth magnitude (high: $h_l = 0.05$ or low: $h_l = 0.01$) specified separately. The last column (%sel) signifies % of datasets for which the best fit model had the lowest DIC and were used to get these results.

True model (Bandwidth)	Selected model	True value	EST	SD	SD_{EST}	%sel	
$A \rightarrow BC-k^{(G)}$ (low)	$A \rightarrow BC-k^{(G)}$	α_2	2	2.03	0.13	0.12	
		α_3	1.5	1.51	0.11	0.10	
		h_2	0.01	0.01	<0.01	<0.01	100
		h_3	0.01	0.01	<0.01	<0.01	
		λ_1^C	150	128.06	11.25	12.37	
$A \rightarrow BC-k^{(G)}$ (high)	$A \rightarrow BC-k^{(G)}$	α_2	2	2.01	0.13	0.13	
		α_3	1.5	1.52	0.11	0.13	
		h_2	0.05	0.05	<0.01	<0.01	81 [†]
		h_3	0.05	0.05	<0.01	0.01	
		λ_1^C	150	126.36	11.17	11.70	
$A \rightarrow BC-k^{(C)}$ (low)	$A \rightarrow BC-k^{(C)}$	α_2	2	2.00	0.13	0.13	
		α_3	1.5	1.50	0.11	0.10	
		h_2	0.01	0.01	<0.01	<0.01	100
		h_3	0.01	0.01	<0.01	<0.01	
		λ_1^C	150	127.23	11.21	11.04	
$A \rightarrow BC-k^{(C)}$ (high)	$A \rightarrow BC-k^{(C)}$	α_2	2	2.00	0.15	0.14	
		α_3	1.5	1.50	0.13	0.12	
		h_2	0.05	0.05	0.01	0.01	94*
		h_3	0.05	0.05	0.01	0.01	
		λ_1^C	150	128.87	11.29	10.44	

[†] The configuration $A \rightarrow BC$ was correctly selected for all datasets while the choice of $k^{(C)}$ yielded the best fit for 19% of datasets.

* The configuration $A \rightarrow BC$ was correctly selected for all datasets while the choice of $k^{(G)}$ yielded the best fit for 6% of datasets.

NOTE: Throughout values are based on the model selected most time among the 100 datasets.

5.1 | Quantifying established relationships in dental plaque biofilm image data

5.1.1 | Analysis of whole image data

Hyperparameters and analysis settings

From the $m = 9$ different taxa probed in the human dental plaque sample, we analyzed the data for locations of three offspring taxa, *Streptococcus* (S), *Porphyromonas* (Po) and *Pasteurellaceae* (Pa). The parent taxon for the first two taxa is *Corynebacterium* (C), and for the third taxon, it is *Streptococcus* which itself is an offspring taxon (Figure 1). According to the notation introduced in Section 3.1, the process Y_1 corresponds to *Corynebacterium*, which functions only as a parent taxon ($p = 1$). Y_2 , Y_3 , and Y_4 represent the three offspring processes ($q = 3$) for *Streptococcus*, *Porphyromonas*, and *Pasteurellaceae*, respectively. The corresponding parent processes are $C_2 = Y_1$, $C_3 = Y_1$ (*Corynebacterium* as a parent), and $C_4 = Y_2$ (*Streptococcus* as a parent). The remainder of the taxa were modeled as HPPs. We denote the model as $C \rightarrow SPo; S \rightarrow Pa$, by using the model notation introduced in Section 4.2.2 and the shorthand symbols for the taxa presented earlier here. We use the notations from Section 3.1 to identify parameters to taxa and the notation from 4.2.2 to refer to the whole model. This convention has been used throughout the rest of the paper.

In the MCPP analyses, we set the hyperparameters at $a_Y = b_Y = a_C = b_C = a = b = 0.01$ and σ at 0.97, such that the 99th percentile for the bandwidth parameters was approximately $2.5 \mu\text{m}$. The inclusion of black space, where no taxa are observed, can deflate density estimates and induce spurious spatial correlations. We minimized unnecessary black space by using a convex

TABLE 3 Results of MCPP and NSP analyses of human dental plaque biofilm data: estimates (EST) and uncertainty measures for the offspring density ($\alpha_2, \alpha_3, \alpha_4$), bandwidth (h_2, h_3, h_4), and parent process (λ^C) parameters. For the MCPP model, the estimates are the posterior means, and SD is computed as the posterior standard deviation for each of the parameters. For the NSP model, the estimates are the output of the minimum contrast method. SD is not computed for NSP, as the method does not provide one.

Type	Taxa		MCPP		NSP
			EST	SD	EST
Offspring	<i>Streptococcus</i>	α_2	1.34	0.05	64.12
		h_2	10.96	0.49	10.19
	<i>Porphyromonas</i>	α_3	2.20	0.06	57.07
		h_3	14.14	0.53	5.74
	<i>Pasteurellaceae</i>	α_4	0.42	0.02	16.01
		h_4	4.55	0.30	8.14
Parent	<i>Corynebacterium</i>	λ_1^C	0.02	< 0.01	< 0.01

hull of the observed locations as the analysis window (Supplementary Material, Figure S.2). We also applied the NSP model individually on the three offspring processes, *Streptococcus*, *Porphyromonas* and *Pasteurellaceae*.

Results

For the MCPP, we ran three chains of length 3 million each with the initial 2 million iterations discarded as burn-in samples and the remaining samples thinned to obtain 10,000 posterior samples from each chain. The mixing was good for all the parameters. The estimates are posterior means and standard deviations based on the samples from three chains. The NSP model was run separately for the three offspring taxa by using the `thomas.estK` function in the R package `spatstat`. It uses the minimum contrast method to estimate the parameters and does not return any uncertainty estimates.

The MCPP identified the previously described multilayered arrangement in which *Streptococcus* and *Porphyromonas* cluster around *Corynebacterium* and *Pasteurellaceae* around *Streptococcus*. The MCPP-based bandwidth estimates for *Streptococcus* and *Porphyromonas* clustering around *Corynebacterium* were higher than expected, both above $\sim 10\mu\text{m}$, and for *Pasteurellaceae* around *Streptococcus* it is $4.55\mu\text{m}$ (Table 3). The NSP estimates for the bandwidth parameters involving *Corynebacterium* are lower, while the corresponding offspring density parameters are very high. The estimated parameters from the MCPP are consistent in the sense that the expected count exactly matches the observed counts when rounded to the nearest integer. See the Supplementary Material for other parameter estimates (Table S.3).

The estimated (homogeneous) K -function for *Corynebacterium* was higher than the expected value of πr^2 (Figure S.3, supplementary materials). The clustering behavior of *Streptococcus* and *Porphyromonas* were not evident from the K -function. *Pasteurellaceae* displayed strong clustering behavior based on its K -function (Figure S.3, Supplementary Material).

5.1.2 | Analysis of subsetted image data

Analysis plan

We subset the image in four equal-sized quadrants (Supplementary Materials, Figure S.2) and analyzed data from each quadrant independently. While this ad hoc approach may be insufficient for some applications, testing and applying more optimal sub-setting methods are beyond the scope of this work. The fact that taxa's abundance varied across the quadrants allowed for some comparison of performance (Supplementary Materials, Table S.4). The hyperparameters were set similarly as before, and convex hulls were created for each of the quadrants. We also performed NSP-based analysis of the three offspring taxa separately for each quadrant.

Results

The estimated bandwidth parameters h_2, h_3 and h_4 for the four quadrants ranged between $7.6\text{--}11.2\mu\text{m}$, $7.2\text{--}15.2\mu\text{m}$ and $3.8\text{--}4.6\mu\text{m}$, respectively. The estimated offspring density parameters α_2, α_3 and α_4 were between $1.0\text{--}2.2$, $1.8\text{--}5.0$ and $0.4\text{--}0.6$, respectively. The estimated intensity parameter for *Corynebacterium* was $0.01\text{--}0.02$ per unit area (Table 4). The estimates of intensity parameters for the other taxa varied among the quadrants (Supplementary Table S.5).

TABLE 4 Results of MCPP and NSP analyses of human dental plaque biofilm data: estimates (EST) and uncertainty measures for the offspring density ($\alpha_2, \alpha_3, \alpha_4$), bandwidth (h_2, h_3, h_4), and parent process (λ_1^C) parameters from separate analyses of data from the four quadrants of the image. For the MCPP model, the estimates are the posterior means, and SD is computed as the posterior standard deviation for each of the parameters. For the NSP model, the estimates are the output of the minimum contrast method. SD is not computed for NSP, as the method does not provide one.

Segment	Type	Taxa		MCPP		NSP
				EST	SD	EST
I	Offspring	<i>Streptococcus</i>	α_2	2.22	0.22	9.94
			h_2	8.32	0.56	2.88
		<i>Porphyromonas</i>	α_3	5.05	0.34	24.19
			h_3	7.23	0.50	2.55
		<i>Pasteurellaceae</i>	α_4	0.57	0.08	15.39
			h_4	3.82	0.40	9.39
	Parent	<i>Corynebacterium</i>	λ_1^C	0.01	< 0.01	< 0.01
II	Offspring	<i>Streptococcus</i>	α_2	1.98	0.10	41.89
			h_2	11.23	0.58	7.07
		<i>Porphyromonas</i>	α_3	2.91	0.13	35.43
			h_3	15.21	0.79	4.57
		<i>Pasteurellaceae</i>	α_4	0.36	0.03	10.12
			h_4	4.23	0.46	6.72
	Parent	<i>Corynebacterium</i>	λ_1^C	0.02	< 0.01	< 0.01
III	Offspring	<i>Streptococcus</i>	α_2	1.04	0.08	9.34
			h_2	7.62	0.71	3.36
		<i>Porphyromonas</i>	α_3	1.80	0.11	18.66
			h_3	9.83	0.72	1.92
		<i>Pasteurellaceae</i>	α_4	0.52	0.06	3.78
			h_4	4.50	0.43	2.67
	Parent	<i>Corynebacterium</i>	λ_1^C	0.02	< 0.01	< 0.01
IV	Offspring	<i>Streptococcus</i>	α_2	1.22	0.08	32.29
			h_2	9.41	0.81	5.84
		<i>Porphyromonas</i>	α_3	2.11	0.11	51.56
			h_3	11.09	0.72	4.14
		<i>Pasteurellaceae</i>	α_4	0.46	0.05	9.93
			h_4	4.62	0.42	4.42
	Parent	<i>Corynebacterium</i>	λ_1^C	0.02	< 0.01	< 0.01

The estimates for the parent intensity and offspring density parameters varied among quadrants and among parent-offspring pairs. The estimates for λ_1^C in each quadrant were consistent with the observed counts. For example, in the second quadrant, there were 219 observed *Corynebacterium* cells, and the estimated intensity parameter was 0.02 per unit area, giving an expected count of ≈ 219 . For each of the three offspring taxa, the estimated counts matched the observed counts when rounded to the nearest integer. For example, the estimated taxon counts for *Streptococcus*, *Porphyromonas* and *Pasteurellaceae* in the third quadrant compute to 163, 269 and 76 respectively, which match the corresponding observed counts (Supplementary Table S.4).

The estimated bandwidth parameters h_2, h_3 and h_4 also varied by quadrant, exhibiting consistent patterns for different offspring-parent pairs. The NSP analysis of each of the offspring processes resulted in very low estimated bandwidth parameter values (Table 4).

5.2 | Application of the MCPP to explore proposed relationships in biofilm image data

5.2.1 | Exploration strategy

Here, the goal was to investigate the plausibility of newly proposed parent-offspring-like clustering relationships by comparing the model fit when they are included with the fit of the original model developed based on prior knowledge, described in Section 5.1. The latter included specific configurations of *Corynebacterium*, *Streptococcus*, *Porphyromonas* and *Pasteurellaceae*. We investigated two relationships that have been reported and not confirmed. First, we fit models to evaluate a potential clustering relationship involving *Streptococcus* around *Fusobacterium* (F)³². Second, we fit models to evaluate different possible clustering configurations of *Fusobacterium* with *Leptotrichia* (L).⁸ observed that the two genera tend to occupy the same area of the biofilm. How they may relate to each other spatially, if at all, is yet unexplored.

5.2.2 | Hyperparameters and analysis settings

Using the notation in Section 4.2.2, we explored the following models:

- | | |
|---|---|
| 1. $C \rightarrow SPo ; S \rightarrow Pa$ | 5. $C \rightarrow SPo ; S \rightarrow Pa ; L \rightarrow F$ |
| 2. $C \rightarrow Po ; F \rightarrow S ; S \rightarrow Pa$ | 6. $C \rightarrow SPo ; S \rightarrow Pa ; F \rightarrow LS$ |
| 3. $C \rightarrow SPo ; F \rightarrow S ; S \rightarrow Pa$ | 7. $C \rightarrow SPo ; S \rightarrow Pa ; L \rightarrow F ; F \rightarrow S$. |
| 4. $C \rightarrow SPo ; S \rightarrow Pa ; F \rightarrow L$ | |

In contrast to the models previously fit, the series of models in this substudy differ in the number of parent and offspring processes. The number of processes that serve only as parent (p) can be 1 (Model 1) or 2 (Models 2 through 7), while the number of unique offspring processes (q) can be 3 (Models 1,2 and 3) or 4 (Models 4 through 7). The choice for hyperparameters $a_Y = b_Y = a_C = b_C = a = b = 0.01$ and σ at 0.97 remains the same with the same reasoning for their choice.

5.2.3 | Results

In this substudy involving serial fitting of models with different configurations, the lowest DIC values, $\sim 124,000$, were from Models 4 and 5, configurations that included *Fusobacterium* and *Leptotrichia* in addition to the well-established configurations around *Corynebacterium* (Supplementary Table S.6). These values were lower than $\sim 125,000$, the DIC of the “base model” that included only the previously known configurations (Model 1). The substudy provided little, if any, support for the proposed clustering of *Streptococcus* around *Fusobacterium* instead of *Streptococcus* around *Corynebacterium* (Model 2), as the DIC, $\sim 125,500$, was higher than that for the base model. And, when *Streptococcus* was assumed to cluster around both *Corynebacterium* and *Fusobacterium* (Models 3, 6, and 7), the DIC values, all $> 133,000$, were by far the highest among the seven models.

The best-fitting model, Model 5 differed from the “base model” only in the addition of a clustering relationship of *Fusobacterium* and *Leptotrichia*. The estimates and the standard deviations for the relationships common to both models were nearly the same. The estimated number of *Fusobacterium* cells per *Leptotrichia* cell is < 1 , and the estimated bandwidth is roughly $5.22 \mu\text{m}$ (Table 5).

6 | DISCUSSION AND CONCLUSION

We have developed a multivariate model to make inference, simultaneously, about multiple parent-offspring clustering relationships, including multiple layers of clustering. The proposed MCPP framework produces model parameters that directly quantify multiple structural arrangements, in which locations of one type of object depend on locations of another, central object. This task cannot be achieved with a traditional NSP approach because it ignores the locations of central “parent” objects. Because the MCPP assumes conditional independence, its use for modeling taxa individually will produce the same parameter estimates as the joint model. An advantage of the joint model over individual models is the ability to compare DIC values for parameterizations in which a set of taxa are modeled in different configurations. Indeed, we demonstrated that comparison of DIC values after serially fitting various MCPP model specifications is especially useful to explore possible clustering relationships when little is known *a priori*.

TABLE 5 Parameter estimates (EST) and uncertainty quantification (SD) for the model best fit according to lowest DIC (Model 5). Parameter estimates are obtained by considering the posterior mean and SD computed by posterior standard deviation. α or h subscripted by 3, 4, 5 and 6 refer to the offspring density and bandwidth parameters for *Streptococcus*, *Porphyromonas*, *Pasteurellaceae* and *Fusobacterium* respectively. The parameters λ_1 and λ_2 represent the intensity parameter for the two parent species *Corynebacterium* and *Leptotrichia* respectively.

Type	Taxon		EST	SD	
Offspring	<i>Streptococcus</i>	α_3	1.33	0.04	
		h_3	10.79	0.47	
	<i>Porphyromonas</i>	α_4	2.19	0.06	
		h_4	14.16	0.60	
	<i>Pasteurellaceae</i>	α_5	0.42	0.02	
		h_5	4.33	0.26	
		<i>Fusobacterium</i>	α_6	0.57	0.02
			h_6	5.22	0.32
Parent	<i>Corynebacterium</i>	λ_1^C	0.02	< 0.01	
	<i>Leptotrichia</i>	λ_2^C	0.03	< 0.01	

In simulation studies, MCPP models correctly identified parent-offspring-type relationships and produced less bias and much lower empirical standard deviations for parameter estimates compared with NSP models, which produced rather nonsensical results. One seeming departure from ideal performance was that the MCPP did not always identify the kernel used to generate data, especially in high-bandwidth scenarios. This is not surprising because tail behaviors are similar for a low-bandwidth Cauchy kernel and a high-bandwidth Gaussian kernel. More importantly, MCPP performance was robust to the choice of kernel.

Although development of the proposed MCPP model was motivated by oral microbiome biofilm image data, the approach is not specific to biofilms. The MCPP can be used in any image applications in which spatial dependencies reflect and provide information about the function of spatially arranged cells (or other objects) or about the function of arrangements themselves (e.g., the relationship between resprouters and seeders in a biodiverse plant community, as taken up by¹⁹).

We demonstrated feasibility and utility of the proposed method in application to biofilm image data that exhibit complex arrangements with nine taxa. Broadly speaking, the MCPP successfully captured the multilayered corn-cob-like structure among a group of four taxa. Additionally, application of the MCPP for data exploration provided evidence to support clustering between *Fusobacterium* and *Leptotrichia*. Because the DICs were nearly the same for models including either $L \rightarrow F$ or $F \rightarrow L$, the data support that they occupy the same physical niche in the biofilm rather than that one clusters around the other. We hope this observation will prompt further study of this previously unexplored relationship.

For some of the well-established clustering arrangements, the estimated bandwidth parameters were much greater than the approximately sub 5-micron distances expected from cell-to-cell (or nearly cell-to-cell) contact apparent in the visible corn-cob arrangements and likely when cells physico-chemically interact. Because of this seeming discrepancy, it could be tempting to conclude that the low parent-offspring bandwidths estimated by the NSP make the NSP a more valid and preferred approach than the MCPP. However, because the classical NSP model ignores the location of parent cells, it highly underestimated the number of cluster centers (“parent” cells). To compensate, it greatly overestimated the offspring density. Additionally, in ignoring parent locations, the NSP models self-cluster instead of parent-offspring clustering. Therefore, though seemingly appealing, the NSP produces estimates that are not appropriate to quantify the multilayered intertaxon relationships we sought to investigate.

It would also be inappropriate to interpret the MCPP’s high average estimated parent-offspring bandwidth strictly as bias or as reflecting a universal drawback to the proposed approach. Rather, the seeming discrepancy suggests the need for careful interpretation of model parameters from such a complex, heterogeneous image. It also highlights a need for modifications to the approach if a simple, direct interpretation about cell-to-cell (parent-to-offspring) contact is the goal.

Two characteristics of the dental plaque biofilm data present particular challenges. First, cells of *Corynebacterium* are filamentous. When the locations of imputed centroids are used to estimate average distances to neighboring cells of a different taxon, centroid-based methods may give misleading estimates of true cell-to-cell distances. This form of bias may be exacerbated by the specific biological organization, in that the spherical offspring taxa (*Streptococcus* and *Porphyromonas*) cluster around only one end of the parent *Corynebacterium* filaments. Estimates of average *Pasteurellaceae*-*Streptococcus* distances

were much smaller and closer to the expected range for cell-to-cell contact, likely because these clusters involved two types of similarly sized, spherical organisms.

One way to improve the MCPP performance, therefore, might be to model the shapes of cells by bi-axial spheroids³³ or elliptical cluster processes³⁴. Another might be to use outline-based approaches, such as the Hausdorff distance³⁵, rather than relying on the geographic coordinates of imputed centroids to locate each filamentous cell. Nevertheless, such complicated adaptations of the MCPP approach are likely to be unnecessary if qualitative inference about the clustering arrangement suffices. Another option we are exploring is to condition models on features empirically identified in the image. Limiting the MCPP analysis only to parent or offspring cells within some short distance of each other (e.g., radius = 10 μm) might improve its usefulness in similar applications, compared with analyses yielding only marginal bandwidth estimates over a heterogeneous spatial structure.

To explore another challenging feature, higher-order spatial structure, we analyzed subsetted image data. Between-quadrant variability in parameter estimates from both the MCPP and NSP methods suggests the subsetting approach was helpful. Even more powerful would be incorporation of the MCPP into a broader modeling framework that could capture higher-order spatial structure, for example, through regression parameters. The proposed model in (1) is flexible in that it can accommodate different standard modeling frameworks. For example, one can choose the form of $\lambda_i(\mathbf{s})$, $i = 1, \dots, m$, and replace the HPP components in (1) by multivariate log-Gaussian Cox process components. Such an extension would enable the characterization and quantification of more complex spatial correlation structures among multiple taxa or other types of objects. We are currently developing these models.

We are also pursuing an avenue that will further enhance usefulness of the approach, by developing a meta-analytic framework to combine data from multiple images. In 100 sampled images of tongue biofilm from five donors, both within-sample and across-sample variability of inter-taxon spatial relationships is apparent³⁶. This variability can be quantified via a meta-analytic, multivariate, log-Gaussian Cox process model. To date, it has not been standard to apply formal unified models to combine data across multiple biomedical images. Instead, most practitioners have relied on post hoc comparisons, such as through ANOVA or non-parametric two-group comparisons. An efficient meta-analytic approach would also allow estimation and testing of covariate relationships with specific spatial structures, thereby increasing the scope and applicability of the proposed method.

Validation of MCPP models is not straightforward. Complex spatial structures generally do not permit out-of-sample prediction or split-sample cross-validation. In the context of traditional Bayesian point process models, the empirical spatial distributions can be compared with those based on posterior predictive samples³⁷. However, this observed-versus-expected approach is challenged by the complexity of the data. Residuals for each of the sub-processes in (1) are easily obtained. Yet, a good match of observed and expected counts for one process can be misleading about overall model fit if another process is poorly estimated. This is exactly what happened with the NSP analysis of real data, where predicted offspring counts were accurate, and predicted parent counts were grossly underestimated. In contrast, the MCPP models produced nearly perfect prediction of counts of different taxa in the observation window. To our knowledge, there is as yet no valid method to combine the multiple residuals to produce a summary statistic reflecting overall goodness-of-fit. Using the DIC as a means to compare fit is valid only when the same method is used across the models.

We have proposed a novel MCPP method for simultaneously quantifying multilayer, multivariate spatial relationships that we applied to explore, confirm, and quantify spatial arrangements of microbial cells in dental plaque biofilm image data. The proposed method exploits information about locations of objects at the center of a cluster of unlike objects, providing distinct advantages over the classic NSP model when information about locations of central “parent” objects is available. The MCPP model clearly outperformed the existing cluster point process model in every scenario in numerical studies.

SUPPLEMENTARY MATERIAL AND SOFTWARE

Supplementary file with more images, tables and details about the method is supplied. R-package MCPP containing code to apply the method is available on request.

ACKNOWLEDGEMENTS

The authors were funded by NIH grants GM126257, DE026872, DE027486, ES000002, DE016937 and DE022586. We are grateful for this support.

References

1. Yates M, Miller L, Peacock J. The cluster environments of powerful, high-redshift radio galaxies. *Mon Not R Astron Soc* 1989; 240(1): 129–166.
2. Hill GJ, Lilly SJ. A change in the cluster environments of radio galaxies with cosmic epoch. *The Astrophysical Journal* 1991; 367: 1–18.
3. Tarof SA, Ratcliffe LM. Habitat characteristics and nest predation do not explain clustered breeding in Least Flycatchers (*Empidonax minimus*). *The Auk* 2004; 121(3): 877–893.
4. Fritzschn B, Dillard M, Lavado A, Harvey NL, Jahan I. Canal cristae growth and fiber extension to the outer hair cells of the mouse ear require Prox1 activity. *PLoS one* 2010; 5(2): e9377.
5. Molnar C, Gair J. *Concepts of biology*. BCcampus . 2015.
6. Gideon HP, Phuah J, Junecko BA, Mattila JT. Neutrophils express pro-and anti-inflammatory cytokines in granulomas from Mycobacterium tuberculosis-infected cynomolgus macaques. *Mucosal immunology* 2019; 12(6): 1370–1381.
7. Jones SJ. A special relationship between spherical and filamentous microorganisms in mature human dental plaque. *Archives of Oral Biology* 1972; 17(3): 613–IN27.
8. Mark Welch JL, Rossetti BJ, Rieken CW, Dewhirst FE, Borisy GG. Biogeography of a human oral microbiome at the micron scale. *Proc Natl Acad Sci* 2016; 113(6): E791–E800.
9. Vorregaard M. Comstat2-a modern 3D image analysis environment for biofilms. Master's thesis. Technical University of Denmark, DTU, DK-2800 Kgs. Lyngby, Denmark. : 2008.
10. Hartmann R, Jeckel H, Jelli E, et al. Quantitative image analysis of microbial communities with BiofilmQ. *Nature microbiology* 2021; 6(2): 151–156.
11. Møller J, Syversveen AR, Waagepetersen RP. Log gaussian cox processes. *Scand. J. Stat.* 1998; 25(3): 451–482.
12. Neyman J, Scott EL. Statistical approach to problems of cosmology. *J R Stat Soc B* 1958; 20(1): 1–29.
13. Møller J. Shot noise Cox processes. *Advances Appl Probab* 2003; 35(3): 614–640.
14. Berman M. Testing for spatial association between a point process and another stochastic process. *J R Stat Soc B* 1986; 35(1): 54–62.
15. Grabarnik P, Särkkä A. Modelling the spatial structure of forest stands by multivariate point processes with hierarchical interactions. *Ecological Modelling* 2009; 220(9-10): 1232–1240.
16. Diggle PJ, Moraga P, Rowlingson B, Taylor BM. Spatial and spatio-temporal log-Gaussian Cox processes: extending the geostatistical paradigm. *Statistical Science* 2013; 28(4): 542–563.
17. Tanaka U, Ogata Y. Identification and estimation of superposed Neyman–Scott spatial cluster processes. *Ann Inst Stat Math* 2014; 66(4): 687–702.
18. Jalilian A, Guan Y, Mateu J, Waagepetersen R. Multivariate product-shot-noise Cox point process models. *Biometrics* 2015; 71(4): 1022–1033.
19. Illian JB, Møller J, Waagepetersen RP. Hierarchical spatial point process analysis for a plant community with high biodiversity. *Environmental and Ecological Statistics* 2009; 16(3): 389–405.
20. Schindelin J, Arganda-Carreras I, Frise E, et al. Fiji: an open-source platform for biological-image analysis. *Nature methods* 2012; 9(7): 676–682.
21. Morillo-Lopez V, Sjaarda A, Islam I, Borisy GG, Mark Welch JL. Corncob structures in dental plaque reveal microhabitat taxon specificity. *Microbiome* 2022; 10(1): 145.

22. Chiu SN, Stoyan D, Kendall WS, Mecke J. *Stochastic geometry and its applications*. John Wiley & Sons . 2013.
23. Ripley BD. *Spatial statistics*. John Wiley & Sons . 2005.
24. Baddeley AJ, Møller J, Waagepetersen R. Non-and semi-parametric estimation of interaction in inhomogeneous point patterns. *Stat Neerl* 2000; 54(3): 329–350.
25. Ripley BD. Modelling spatial patterns. *J R Stat Soc B* 1977; 39(2): 172–192.
26. Moller J, Waagepetersen RP. *Statistical inference and simulation for spatial point processes*. CRC Press . 2003.
27. Diggle PJ. *Statistical analysis of spatial and spatio-temporal point patterns*. CRC press . 2013.
28. Kopecký J, Mrkvička T. On the Bayesian estimation for the stationary Neyman-Scott point processes. *Applications of Mathematics* 2016; 61(4): 503–514.
29. Green PJ. Reversible jump Markov chain Monte Carlo computation and Bayesian model determination. *Biometrika* 1995; 82(4): 711–732.
30. Spiegelhalter DJ, Best NG, Carlin BP, Van Der Linde A. Bayesian measures of model complexity and fit. *J R Stat Soc B* 2002; 64(4): 583–639.
31. Baddeley A, Rubak E, Turner R. *Spatial point patterns: methodology and applications with R*. CRC press . 2015.
32. Lancy Jr P, Dirienzo J, Appelbaum B, Rosan B, Holt S. Corncob formation between *Fusobacterium nucleatum* and *Streptococcus sanguis*. *Infection and immunity* 1983; 40(1): 303–309.
33. Clem C, Boysen M, Rigaut J. Towards 3-D modelling of epithelia by computer simulation.. *Anal. Cell. Pathol.* 1992; 4(4): 287–301.
34. Meinhardt M, Lück S, Martin P, et al. Modeling chondrocyte patterns by elliptical cluster processes. *J. Struct. Biol.* 2012; 177(2): 447–458.
35. Huttenlocher DP, Klanderman GA, Rucklidge WJ. Comparing images using the Hausdorff distance. *IEEE Trans Pattern Anal Mach Intell* 1993; 15(9): 850–863.
36. Wilbert SA, Welch JLM, Borisy GG. Spatial ecology of the human tongue dorsum microbiome. *Cell reports* 2020; 30(12): 4003–4015.
37. Leininger TJ, Gelfand AE. Bayesian inference and model assessment for spatial point patterns using posterior predictive samples. *Bayesian Analysis* 2017; 12(1): 1–30.

How to cite this article: S. Majumder, B. A. Coull, J. L. Mark Welch, P. J. La Riviere, F. E. Dewhirst, J.R. Starr, and K. Lee (2024), Multivariate cluster point process to quantify and explore multi-entity configurations: Application to biofilm image data, *Stat. In Medicine*, 2024;00:1–6.